

We are IntechOpen, the world's leading publisher of Open Access books Built by scientists, for scientists

6,900

Open access books available

186,000

International authors and editors

200M

Downloads

Our authors are among the

154

Countries delivered to

TOP 1%

most cited scientists

12.2%

Contributors from top 500 universities



WEB OF SCIENCE™

Selection of our books indexed in the Book Citation Index
in Web of Science™ Core Collection (BKCI)

Interested in publishing with us?
Contact book.department@intechopen.com

Numbers displayed above are based on latest data collected.
For more information visit www.intechopen.com



Selective Control Information Detection in 5G Frame Transmissions

Saheed A. Adegbite and Brian G. Stewart

Additional information is available at the end of the chapter

<http://dx.doi.org/10.5772/66256>

Abstract

Control signalling information within wireless communication systems facilitates efficient management of limited wireless resources, plays a key role in improving system performance of 5G systems. This chapter focuses detection of one particular form of control information, namely, selective control information (SCI). Maximum-likelihood (ML) is one of the conventional SCI detection techniques. Unfortunately, it requires channel estimation, which introduces some implementation constraints and practical challenges. This chapter uses generalized frequency division multiplexing (GFDM) to evaluate and demonstrate the detection performance of a new form of SCI detection that uses a time-domain correlation (TDC) technique. Unlike the ML scheme, the TDC technique is a form of blind detection that has the capability to improve detection performance with no need for channel estimation. In comparison with the ML based receiver, results show that the TDC technique achieves improved detection performance. In addition, the detection performance of the TDC technique is improved with GFDM receivers that use the minimum mean square error (MMSE) scheme compared with the zero-forcing (ZF) technique. It is also shown that the use of a raised cosine (RC) shaped GFDM transmit filter improves detection performance comparison with filters that employ root raised cosine (RRC) pulse shape.

Keywords: 5G frame, blind detection, generalised frequency division multiplexing (GFDM), minimum mean square error (MMSE), physical control channel

1. Introduction

New physical layer architecture developments are under consideration for future 5G wireless systems to meet growing demands for even higher data rates and increasing data traffic. In comparison with the classical orthogonal frequency division multiplexing (OFDM) used in 4G, 5G physical layer architectures adopt a new type of frequency division multiplexing based on filtered OFDM in an attempt to improve spectral efficiency, increase data throughput and

reduce latency [1]. In addition, 5G systems are designed to enable flexible resource allocation and configurable system architecture based on various communication scenarios, varied traffic and user needs [2]. To meet these challenges, various forms of system-critical control information are required to be transmitted through the use of both shared and dedicated physical control channels to facilitate efficient management of 5G system resources and to achieve optimum system performance. This chapter discusses and describes the use of a time-domain blind detection technique that uses time-domain correlation (TDC) between the transmitted control information and the received control information as a means of detection.

Control signals are important in wireless systems as they carry essential signalling information between the user equipment (UE) and the base station to facilitate successful detection of payload user data. Hence, successful detection of these control signals is a key to achieving the required system performance in 5G systems. In general, 5G control signals carry both user-specific and network-level information such as scheduling grant, user allocation, adaptive modulation and coding schemes (AMC), 5G frame configuration and power control. In practical wireless systems, an erroneous detection of control signals triggers re-transmission and causes transmission delays, which will ultimately degrade system performance. As a consequence, control signals are normally encoded using a large number of subcarriers to ensure robust and error-free detection [3].

The focus of this chapter is to address detection challenges of a specific category of wireless control signals called selective control information (SCI). An example of SCI encountered in 4G and implemented in 5G is the control format indicator (CFI) carried by the physical control format indicator channel (PCFICH). The CFI is used to inform the receiver about the signal format of the physical downlink control channel (PDCCH) and is a form of SCI because the actual CFI value ranges between 1 and 4 [3]. Hence, the encoded CFI information can be chosen (i.e. selected) from a small number of candidate CFI information values, which are known at both transmitting and receiving ends of the system [4]. The PDCCH carries major downlink control information (DCI) that represents various types of network configuration and system variables including power control, resource allocations and scheduling grants. A more detailed discussion on CFI can be found in [3]. Another example of SCI is the control information used to encode the type of modulation scheme of payload user data. In summary, SCI is a type of control information that is selective from a deterministic set of candidate information sequences known at both the transmitter and the receiver [5].

In the literature, the maximum likelihood (ML) detection scheme is considered as the standard detection technique for decoding SCI because it is more computationally efficient solution, in terms of hardware implementation, compared with methods such as the K-best list sphere detector (K-LSD) and successive interference cancellation (SIC) [6]. An example of a practical hardware implementation of the ML estimation method for the decoding of the PCFICH is described in [7]. Unfortunately, the ML detection scheme imposes a practical constraint in that it requires channel estimation at the receiver. In theory, the detection performance of the ML estimation technique can be enhanced through the use of an advanced channel estimation technique such as linear minimum mean square error (LMMSE). However, the need for channel estimation requires additional transmission overhead in the form of pilot signals to

facilitate pilot-assisted channel estimation and also increases computational complexity at the receiver. Therefore, the need for channel estimation makes the ML scheme an unattractive and unsuitable solution in practical systems and in the occurrence of severe fading channel [6].

Unlike the ML detection method, the TDC solution discussed in this chapter is a form of blind detection technique in that it requires neither channel estimation nor channel equalisation at the receiver. The TDC technique is designed to address the practical challenges of the ML estimation method and to improve detection performance of essential control signalling information adopted in 5G systems. To demonstrate the potential use of the TDC detection technique in 5G systems and its advantage over the ML detection method, this chapter investigates, through MATLAB simulations, the detection performance of the TDC detection technique using the well-known generalised frequency division multiplexing (GFDM) architecture being considered for 5G. In this study, the detection performance is evaluated using the block error rate (BLER) metric. The effects of GFDM demodulation techniques and transmit filter pulse shapes are studied and investigated to further understand and demonstrate the potential use of the TDC technique in a practical GFDM system. In comparison with the classical OFDM technique, GFDM performs subcarrier-level filtering to minimise or manage out-of-band (OOB) radiation and improve spectral efficiency in 5G. The roll-off factor α of the transmit filter plays a key role towards controlling the OOB. Therefore, the pulse shape and the roll-off factor of the transmit filter will impact detection performance. Using filters with root-raised-cosine (RRC) and raised-cosine (RC) responses, one aspect of this chapter will investigate the dependency between shape of the transmit filter and detection performance of the TDC technique. Another aspect of this chapter will also investigate the influence of the roll-off factor of each chosen filter type on the detection performance.

In practice, GFDM demodulation can be implemented using techniques such as zero-forcing (ZF), minimum mean square error (MMSE) and matched filtering (MF) [2]. In this chapter, only the ZF and MMSE are considered because of the self interference caused by the use of the MF technique. The impact of these two GFDM demodulation methods on the detection performance of the TDC technique is studied so as to further understand and highlight the limitations and/or robustness of the TDC detection technique for 5G systems.

2. SCI Transmission and Reception

This section briefly describes the basic transmitter/receiver architecture used to encode and decode the SCI.

2.1. SCI Transmission

A detailed description of the GFDM transmitter is presented in [2]. **Figure 1** describes a block diagram representation of the considered GFDM transmitter architecture.

Let \mathbf{d} be the transmitted source data of length N , which may consist of control signalling formation, payload user data and some preambles. In GFDM, modulated subcarrier symbols in \mathbf{d} are formatted into a 2D time-frequency GFDM block of dimension K by M where K and M ,

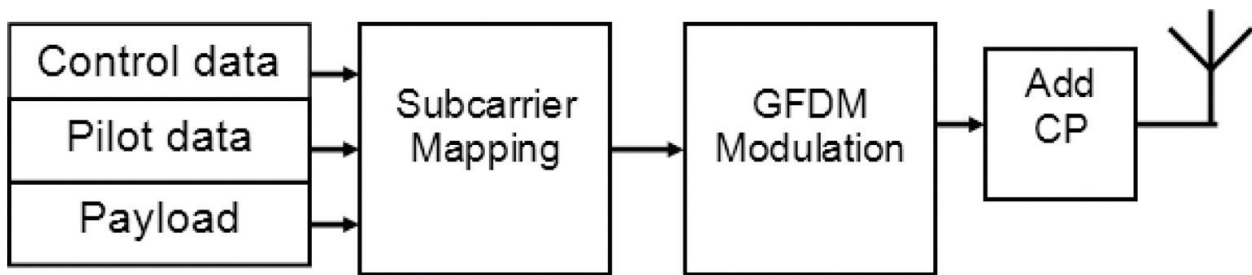


Figure 1. GFDM transmitter.

respectively, represent the number of subcarriers (in the frequency-domain) and the number of subsymbols (in the time-domain) [8]. For $0 \leq k \leq K - 1$ and $0 \leq m \leq M - 1$, where k and m are arbitrary indices of the subcarrier and subsymbol, respectively, each subcarrier symbol in \mathbf{d} can be denoted by $d_{k,m}$ and \mathbf{d} can be represented as

$$\mathbf{d} = [d_{0,0} \ d_{1,0} \ \dots \ d_{K-1,0} \ d_{0,1} \ \dots \ d_{K-1,1} \ d_{k,m} \ \dots \ d_{K-1,M-1}]. \quad (1)$$

2.1.1. Subcarrier mapping

Figure 2 shows a diagrammatic representation of the considered subcarrier mapping scheme. For simplicity, in this chapter, it is assumed that \mathbf{d} consists of (1) a pilot sequence, d_p of size N_p ; (2) an SCI sequence vector, d_c of size N_c ; and (3) other forms of control/payload information, d_r of size N_d . Thus, $N = N_p + N_c + N_d$.

Pilot mapping



Pilot + SCI mapping



Figure 2. Subcarrier mapping.

2.1.1.1. Subcarrier mapping: pilots

In an attempt to mimic practical 5G frame structures, some preambles in the form of reference signals or pilots are embedded with the transmitted signal. In practical systems, reference signals are often adopted to facilitate channel estimation and synchronisation so as to improve data recovery performance of payload user data. Within the considered subcarrier mapping, some pilots are embedded within d at regular intervals. As an example, a pilot spacing of six is considered in this study because currently, there is no standard specification for pilot spacing in 5G.

2.1.1.2. Subcarrier mapping: SCI

After pilot subcarrier allocation, SCI subcarriers are allocated as indicated in **Figure 2**. In the considered mapping, it is assumed that the size of the SCI sequence d_c is a multiple of 4 so that elements of d_c are mapped in groups of 4 in a similar manner to a form of resource element mapping in 4G. The four subcarriers in each group are mapped to un-allocated subcarriers in-between two consecutive pilot positions.

Let \mathcal{C} represent a set of candidate information, which consists of U different SCI sequences, that is,

$$\mathcal{C} = \{\mathbf{C}_1, \mathbf{C}_2, \mathbf{C}_u \dots \mathbf{C}_U\} \quad (2)$$

where each \mathbf{C}_u is of the same size as d_c and each element of \mathbf{C}_u is a complex-valued QPSK-modulated symbol of unity magnitude. For $0 \leq c \leq N_c - 1$, where c is an arbitrary index, each element of \mathbf{C}_u is denoted by $\mathbf{C}_u[c]$. The complex conjugate $\mathbf{C}_u[c]^*$ is mathematically equivalent to $1/\mathbf{C}_u[c]$.

As an example, assume that the encoded SCI is used to carry information about the modulation scheme of payload user data. In the case of 4G and also 5G, there is a finite number of known modulation types and each type can be encoded into an SCI sequence \mathbf{C}_u where $1 \leq u \leq U$. **Table 1** shows an example of the mapping of \mathbf{C}_u to a modulation type. Thus, the transmitted SCI sequence is uniquely identified by the index u given that \mathcal{C} is deterministic and known. Hence, a block-level detection is performed at the receiver in order to determine an estimate of \bar{u} , from which the type of modulation or any other form of control information is automatically determined [9]. It is important to note that a block-level detection procedure

SCI index, u/\bar{u}	SCI, d_c	Modulation
1	\mathbf{C}_1	4-QAM
2	\mathbf{C}_2	16-QAM
3	\mathbf{C}_3	64-QAM
4	\mathbf{C}_4	256-QAM

Table 1. An example of SCI encoding scheme.

used for the recovery of control information is entirely different from the usual subcarrier-level or one-tap equalisation associated with the recovery of payload user data [5].

Given that the transmitted SCI sequence d_c is chosen from a finite set \mathcal{C} , let \bar{u} define the index of the selected and transmitted SCI sequence vector, such that:

$$d_c = C_{\bar{u}} \text{ where } C_{\bar{u}} \in \mathcal{C}. \quad (3)$$

After SCI mapping, all other remaining un-allocated subcarriers are assigned to other forms of data d_r . It is important to note that the main focus of this chapter is on the detection of the SCI index u that corresponds to d_c .

2.1.2. Transmitted signal

Let x be the time-domain GFDM signal of length N . For $0 \leq n \leq N - 1$, each element $x[n]$ is derived from Ref. [2]

$$x[n] = \sum_{k=0}^{K-1} \sum_{m=0}^{M-1} g_{k,m}[n] d_{k,m} \quad (4)$$

where $g_{k,m}[n]$ represents a time and frequency shifted form of a transmit filter $g[n]$. Each $g_{k,m}[n]$ is given as [2]

$$g_{k,m}[n] = g[(n-mK) \bmod N] \exp\left(-j2\pi \frac{k}{K} n\right) \quad (5)$$

where **mod** is the modulo function.

Let A be the transmit filter matrix where

$$A = [g_{0,0} \ g_{1,0} \ \cdots \ g_{K-1,0} \ g_{0,1} \ \cdots \ g_{K-1,1} \ g_{k,m} \ \cdots \ g_{K-1,M-1}]. \quad (6)$$

Then, the GFDM signal can also be expressed by Michailow et al. [2]

$$x = Ad. \quad (7)$$

Finally, the GFDM signal x is further extended by a cyclic prefix (CP) to mitigate channel fading and reduce inter-symbol interference (ISI).

2.2. SCI Detection

In this chapter, SCI decoding is implemented using the ML and the TDC detection techniques. **Figure 3** shows the block diagram representation of the conventional ML-based SCI detection scheme. It is important to note that the considered receiver architecture for decoding SCI is slightly different from typical GFDM receiver for decoding payload user data. For instance, in a typical GFDM receiver, QAM demodulation is required to determine an estimate of

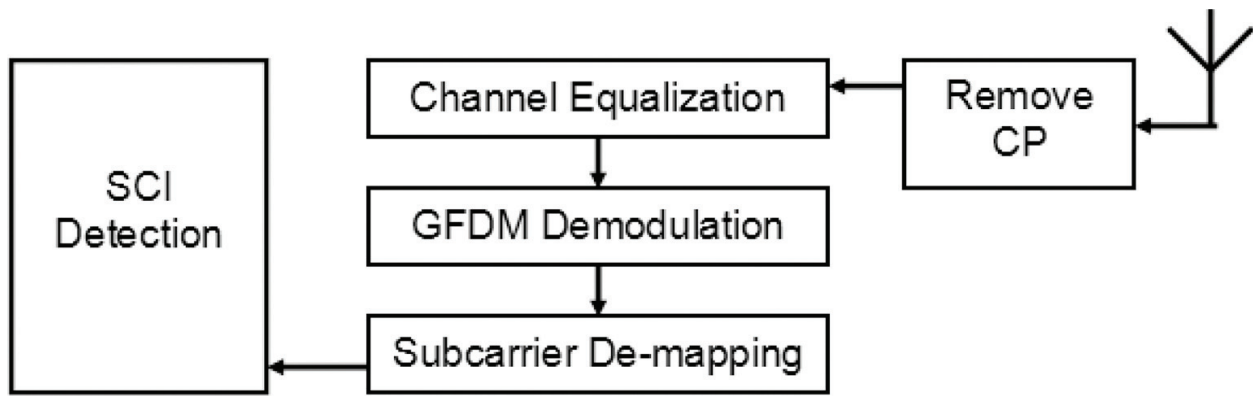


Figure 3. ML-based receiver architecture.

transmitted bitstream. However, in the considered receiver, a form of SCI decoding is implemented instead of QAM demodulation. Unlike QAM demodulation, SCI decoding produces a scalar value that represents an estimate of the SCI index \bar{u} .

After CP removal at the receiver, let \mathbf{y} be the received signal after the transmission over a transmission channel medium with channel matrix \mathbf{H} , corrupted with additive white Gaussian noise \mathbf{v} with variance σ_v^2 , as expressed by Michailow et al. [2], thus

$$\mathbf{y} = \mathbf{H} \mathbf{A} \mathbf{d} + \mathbf{v}. \quad (8)$$

The next stage involves GFDM demodulation, which serves to mitigate the inter-carrier interference (ICI) cause by the filtering process at the transmitter. Let $\hat{\mathbf{B}}$ be a $N \times N$ receiver matrix, which is used for GFDM demodulation.

In the ZF-based GFDM receiver, $\hat{\mathbf{B}}$ is computed using

$$\hat{\mathbf{B}} = (\mathbf{A}^H \mathbf{A}) \mathbf{A}^H \quad (9)$$

where \mathbf{A}^H denotes an Hermitian or conjugate transpose of \mathbf{A} . In the MMSE-based receiver, the receiver matrix $\hat{\mathbf{B}}$ is, however, determined from

$$\hat{\mathbf{B}} = \left(\frac{\sigma_v^2}{\sigma_d^2} \mathbf{I} + \mathbf{A}^H \mathbf{A} \right)^{-1} \mathbf{A}^H. \quad (10)$$

From the expression in Eq. (10), \mathbf{I} is the identity matrix, and σ_d^2 is the variance of \mathbf{d} . Using $\hat{\mathbf{B}}$, the output of the GFDM demodulation block is computed from

$$\hat{\mathbf{d}} = \hat{\mathbf{B}} \mathbf{y}. \quad (11)$$

Hence, the received SCI subcarriers $\hat{\mathbf{d}}_c$ are represented as a subset of $\hat{\mathbf{d}}$. The next stage involves the SCI decoding where an estimate of the index \bar{u} is determined given that the set \mathcal{C} is also

known at the receiver. In this case, the decoded SCI can be directly determined through an estimate of the SCI index \hat{u} .

2.2.1. ML scheme

The ML detection technique uses a form of Euclidean distance minimisation function. Let H_c represent the frequency-domain representation of sub-channel coefficients that correspond to the SCI subcarrier locations.

Let \hat{u} denote an estimate of \bar{u} . Then, using the ML decision criterion, \hat{u} is determined through

$$\hat{u} = \arg \min_{u; C_u \in \mathcal{C}} |\hat{d}_c - H_c C_u|^2. \quad (12)$$

The expression in Eq. (12) suggests that detection performance of the ML estimation method depends on the channel coefficients H_c . In this chapter, the ML decision is implemented using perfect channel estimation. However, in practical systems, channel estimation is implemented as described in [10]. Unfortunately, the need for channel estimation increases both design and computational complexities, and erroneous channel estimation is expected to produce erroneous estimation of \hat{u} . This is the main practical challenge associated with the use of the ML estimation method in 5G wireless systems.

3. TDC Detection Technique

The TDC technique uses a form of signal correlation as a means of detection. A time-domain detection approach is considered because studies from, for example, [11] and [12] have shown that it offers robust decoding even in the presence of ISI [13]. With regard to SCI specifically, the TDC technique uses a correlation that exists between \hat{d}_c and each possible candidate SCI C_u within \mathcal{C} is used to determine an estimate of the transmitted SCI [5]. **Figure 4** shows the block diagram representation of the GFDM receiver that uses the TDC-based SCI detection scheme.

3.1. Discrete Correlation Theorem

The applied correlation within the TDC detection technique can be explained using the well-known discrete correlation theorem (DCT). Based on the DCT, a correlation of two arbitrary time-domain signals q_1 and q_2 (of the same size) is obtained from [14]

$$\text{CORR}\{q_1, q_2\} = \text{IFFT}\{Q_1 \times Q_2^*\} \quad (13)$$

where $*$ represents the complex conjugation, and Q_1 and Q_2 are, respectively, the frequency-domain representations of q_1 and q_2 , that is,

$$Q_1 = \text{FFT}\{q_1\} \quad \text{and} \quad Q_2 = \text{FFT}\{q_2\} \quad (14)$$

where $\text{FFT}\{\cdot\}$ denotes the fast Fourier transform (FFT) function.

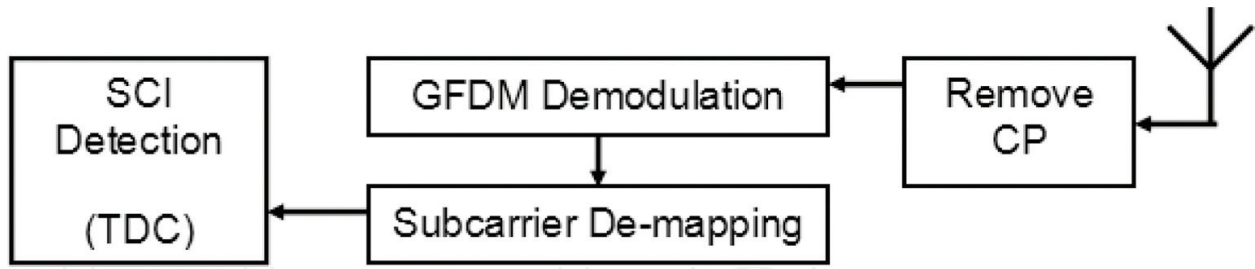


Figure 4. TDC-based receiver architecture.

In a TDC-based receiver, a complex-valued term Z_u is first computed in a similar manner to the DCT definition in Eq. (13). Thus, Z_u is given by

$$\begin{aligned}
 Z_u &= \hat{\mathbf{d}}_c \times \mathbf{C}_u^* \\
 &= (\mathbf{H}_c \hat{\mathbf{d}}_c + \mathbf{V}_c) \times \mathbf{C}_u^* \\
 &= (\mathbf{H}_c \hat{\mathbf{d}}_c \mathbf{C}_u^*) + (\mathbf{V}_c \mathbf{C}_u^*) \\
 &= (\mathbf{H}_c \hat{\mathbf{d}}_c \mathbf{C}_u^*) + (\mathbf{V}'_c(u))
 \end{aligned} \tag{15}$$

where \mathbf{V}_c is the frequency-domain representation of AWGN components of the SCI subcarriers and $\mathbf{V}'_c(u) = \mathbf{V}_c \mathbf{C}_u^*$. For $0 \leq c \leq N_c - 1$, Z_u is a vector of size N_c and may be represented as

$$Z_u = [Z_u[0], Z_u[1], Z_u[c] \dots Z_u[N_c-1]]. \tag{16}$$

When there is a strong correlation between $\hat{\mathbf{d}}_c$ and \mathbf{C}_u , then the expression in Eq. (15) can be approximated to

$$Z_u \approx \begin{cases} \mathbf{H}_c + \mathbf{V}'_c(u), & u = \bar{u} \\ \mathbf{H}_c \hat{\mathbf{d}}_c \mathbf{C}_u^* + \mathbf{V}'_c(u), & \text{otherwise.} \end{cases} \tag{17}$$

By omitting the noise terms in Eq. (17) for simplicity, the expression in Eq. (17) is reduced to

$$Z_u \approx \begin{cases} \mathbf{H}_c, & u = \bar{u} \\ \mathbf{H}_c \hat{\mathbf{d}}_c \mathbf{C}_u^*, & \text{otherwise.} \end{cases} \tag{18}$$

From the expression in Eq. (17), it can be seen that the same channel term \mathbf{H}_c and identical noise term $\mathbf{V}'_c(u)$ are present in both $Z_{u=\bar{u}}$ and $Z_{u \neq \bar{u}}$ terms when $u = \bar{u}$ and $u \neq \bar{u}$, respectively. Thus, without loss of generality, a simplified representation of the main difference between each value of $Z_{u=\bar{u}}$ and $Z_{u \neq \bar{u}}$ is further reduced to

$$Z_u[c] \approx \begin{cases} \mathbf{1}, & u = \bar{u} \\ \hat{\mathbf{d}}_c \mathbf{C}_u^*, & \text{otherwise.} \end{cases} \tag{19}$$

In a similar manner to the expression in Eq. (13), let z_u be the time-domain equivalent Z_u obtained from

$$z_u = \underset{N_c\text{-point}}{\text{IFFT}} \{Z_u\}. \quad (20)$$

In this chapter, z_u will be referred to as the TDC function. For $0 \leq w \leq N_c - 1$, z_u is written as

$$z_u = [z_u[0], z_u[1], z_u[w] \dots z_u[N_c-1]]. \quad (21)$$

It should be noted that the IFFT operation in Eq. (20) requires no zero padding if the value of N_c is a power of 2. However, in cases (not shown in this chapter) where N_c is not a power of 2, zero padding can be applied as required in FFT algorithms with no degradation in performance.

3.2. TDC Decision Criterion

From the approximation of $Z_{\bar{u}}$ in Eq. (19), the magnitudes of $Z_{\bar{u}}$ result in an impulse function in a similar manner to an auto-correlation function. Hence, the magnitude $z_{\bar{u}}[w]$ (derived from $Z_{\bar{u}}$) can be approximated to

$$|z_{\bar{u}}[w]| = \begin{cases} 1, & w = 0 \\ 0, & 1 \leq w \leq N_c - 1 \end{cases} \quad (22)$$

where $|\cdot|$ is the magnitude of a complex-valued variable. Otherwise, $|z_u[w]| > 0$ when $u \neq \bar{u}$.

Using the approximation in Eq. (22), the mean value of $|z_{\bar{u}}|$ is

$$\begin{aligned} E\{|z_{\bar{u}}|\} &= \frac{1}{N_c} \sum_{w=0}^{N_c-1} |z_{\bar{u}}[w]| \\ &\approx 1/N_c \end{aligned} \quad (23)$$

where \mathbf{E} is the expectation function. Similarly, from the definition in Eq. (22), $E\{|z_{u \neq \bar{u}}|\}$ is expected to be larger than $E\{|z_{\bar{u}}|\}$ because the corresponding magnitudes of $z_{u \neq \bar{u}}[w]$ are non-zero. Therefore,

$$E\{|z_{\bar{u}}|\} \ll E\{|z_{u \neq \bar{u}}|\}. \quad (24)$$

Thus, in the presence of the channel fading term H_c , the expression in Eq. (24) is still valid since the resulting time-domain functions $z_{\bar{u}}$ and $z_{u \neq \bar{u}}$ are both affected by the same channel component.

The expression in Eq. (24) therefore implies that an estimate of \bar{u} corresponds to the u -index of the time-domain function with the minimum mean value amongst all U time-domain functions. Therefore, the TDC detection criterion is defined by Saheed et al. [5]

$$\hat{u} = \underset{u}{\arg \min} E\{|z_u|\}. \quad (25)$$

From the expressions in Eqs. (15)–(25), it can be noted that the TDC detection technique requires no channel estimation. The main potential drawback of the TDC technique is the need

for multiple IFFTs, which may increase computational complexity of the TDC-based receiver, particularly in limited practical cases, where the number of candidate SCI U is large. However, this may not be a critical problem due to increased use of high-speed digital signal processors (DSPs) with efficient implementation of FFT.

3.3. Rayleigh Distribution

The hypothesis in Eq. (25) suggests that the distribution of $|z_u|$ may follow a Rayleigh distribution. Let x be a continuous random variable. By letting $x = |z_u[w]|$, the Rayleigh probability distribution function (PDF) of x can be described by Walck [15]

$$P(x) = \frac{x}{\lambda^2} \exp(-x^2/2\lambda^2), x > 0 \quad (26)$$

where λ is the Rayleigh scale parameter, which indicates the point (the value of x) at which the PDF $P(x)$ is maximum [15]. As a function of λ , the mean of x , $E(x)$, is expressed by Walck [15]

$$E(x) = \lambda \sqrt{\frac{\pi}{2}}. \quad (27)$$

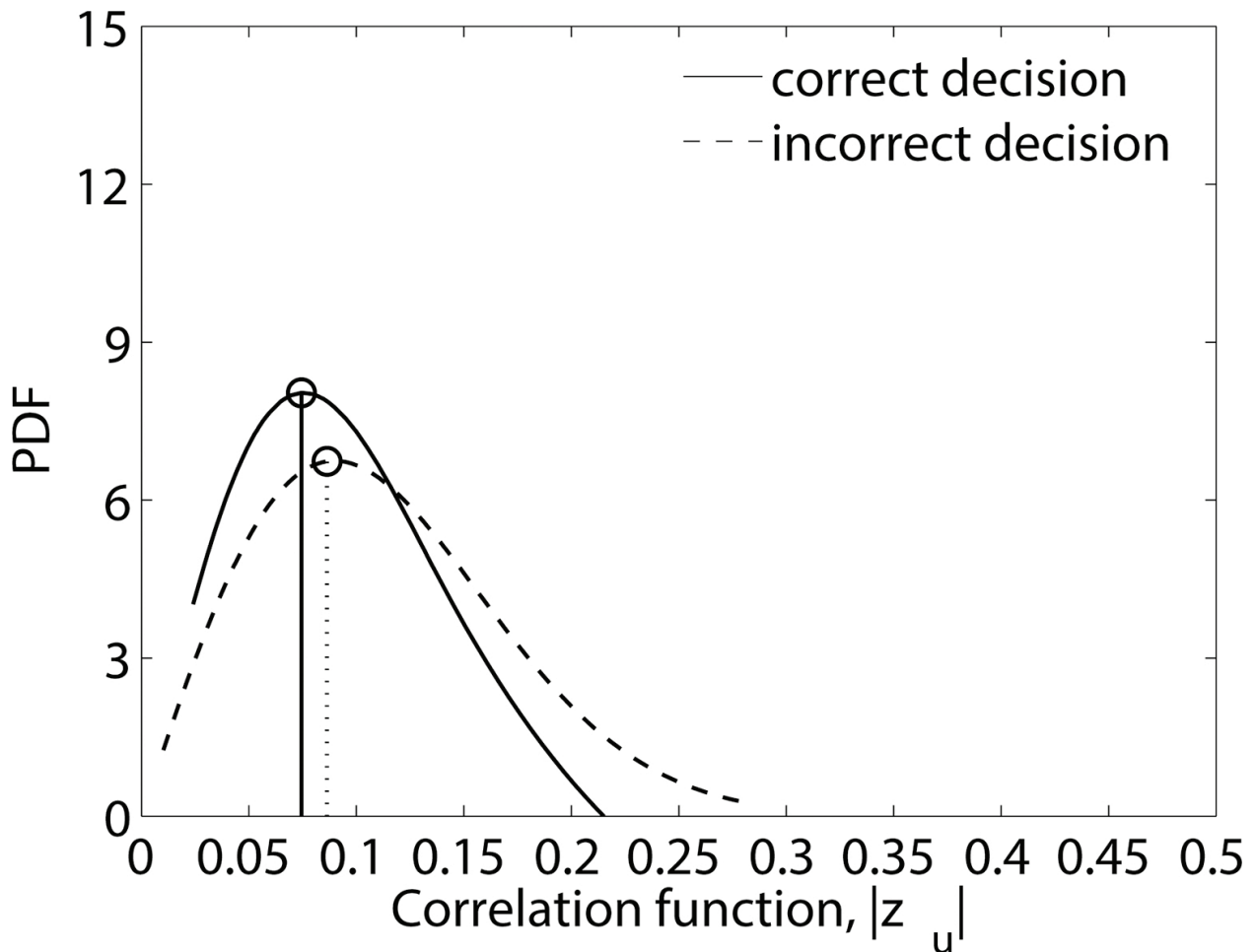


Figure 5. Distribution of $|z_u|$.

The expression for $E(x)$ indicates a linear relationship between λ and $E(x)$. Hence, in relation to the TDC decision criterion in Eq. (25), the value of λ is expected to be smaller for a correct decision compared with the case of an incorrect decision. As an example, **Figure 5** shows the Rayleigh PDF of $|z_u|$ in the presence of a multipath channel fading and transmit signal-to-noise ratio (SNR) of 6 dB. Results in **Figure 5** indicate that the value of λ is smaller when $u = \bar{u}$ compared with when $u \neq \bar{u}$. Therefore, amongst all the U correlation functions, the TDC-based decision criterion minimises the mean of $|z_u|$.

4. Detection Performance

This section presents the numerical detection performance of the TDC detection technique in comparison with the ML scheme. MATLAB simulations demonstrate the effect of the GFDM demodulation technique and the filter pulse shape characteristics on the detection performance of the TDC technique.

4.1. Simulation Set-up

Simulations consider that a GFDM system with $K = 64$, $M = 9$, $N_c = 32$, $U = 4$ and the size of CP is set to 16. Simulation is based on transmission over a frequency-selective Rayleigh fading channel known as the extended pedestrian type A (EPA), with a root mean square (RMS) delay spread, τ_{rms} of 45ns [16]. **Table 2** shows the power-delay profile of the EPA channel [17].

Channel parameters	1	2	3	4	5	6	7
Path delay, ns	0	30	70	90	110	190	410
Power, dB	0.0	-1.0	-2.0	-3.0	-8.0	-17.2	-20.8

Table 2. EPA fading channel.

4.1.1. Block error rate

For user data, bit error rate (BER) is often used as the detection performance metric. However, in the case of control information, the BLER is the customary detection performance metric [5]. To compute the BLER, an error count between the actual value \bar{u} that corresponds to the selected sequence d_c and its estimate \hat{u} obtained at the receiver is evaluated. An erroneous block exists when $\bar{u} \neq \hat{u}$. Otherwise, the detection is considered error-free.

For each SNR level, the BLER is computed as [5]

$$\text{BLER} = \frac{1}{N_{\text{BLK}}} \sum_{i=1}^{N_{\text{BLK}}} F_i \quad (28)$$

where N_{BLK} is the number of OFDM symbol blocks (for a given SNR level). For $1 \leq i \leq N_{\text{BLK}}$, F_i is computed from

$$F_i = \begin{cases} 1 & \text{if } \bar{u} \neq \hat{u} \\ 0 & \text{otherwise.} \end{cases} \quad (29)$$

The BLER produced by each SCI decoding technique is evaluated as a function of the GFDM demodulation technique, filter type and filter roll-off factor parameter. The frequency-domain response of the considered RC filter with a roll-off factor α is given by Michailow et al. [2]

$$G_{RC}[f] = \frac{1}{2} \left[1 - \cos \left(\pi \text{lin}_\alpha \left(\frac{f}{M} \right) \right) \right]. \quad (30)$$

Thus, the frequency-domain response of the RRC filter response is derived as

$$G_{RRC}[f] = \sqrt{G_{RC}[f]}. \quad (31)$$

4.2. Numerical Results

4.2.1. Detection performance with ZF-based GFDM receiver

Using the ZF-based GFDM demodulation technique, **Figure 6** shows the BLER performance of the TDC technique based on an RRC shaped filter with roll-off factor of 0.1, 0.5 and 0.9.

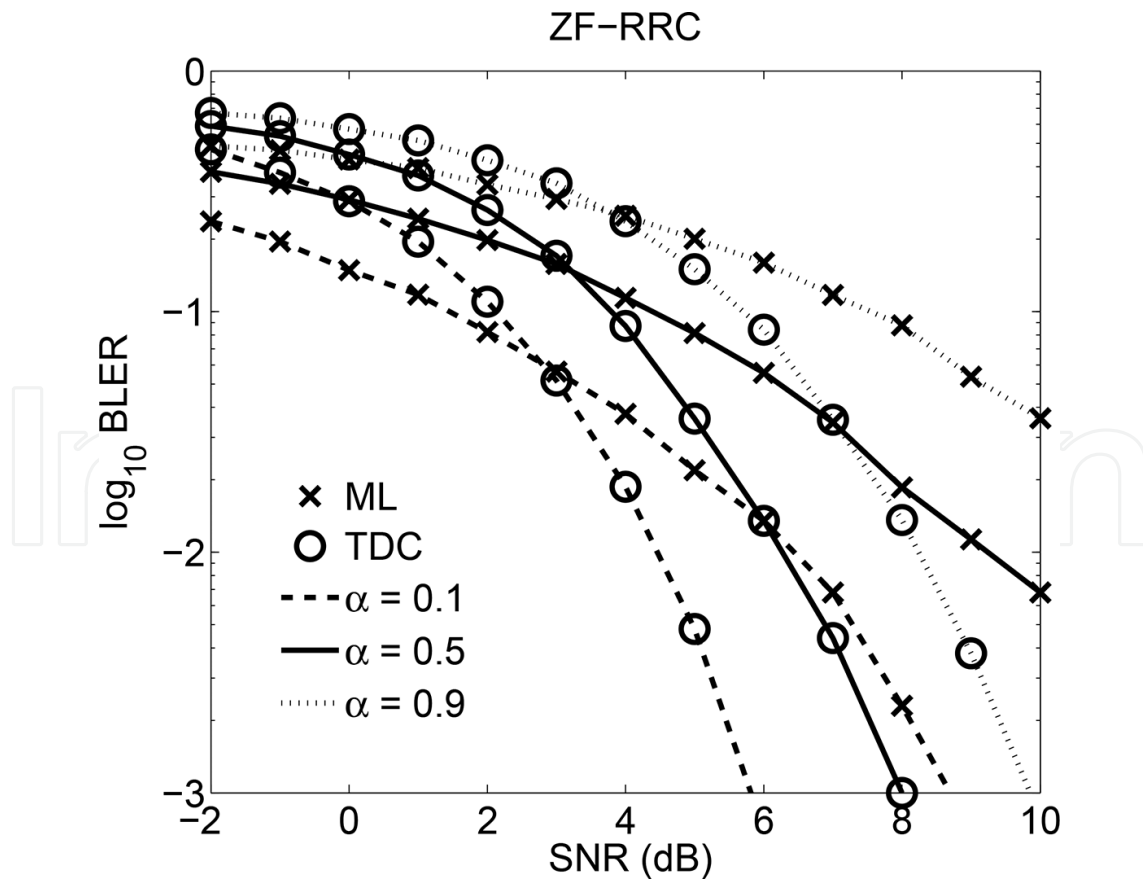


Figure 6. BLER comparison of the ML/TDC techniques with ZF, RRC shaped filter and roll-off factor $\alpha = [0.1, 0.5 \text{ and } 0.9]$.

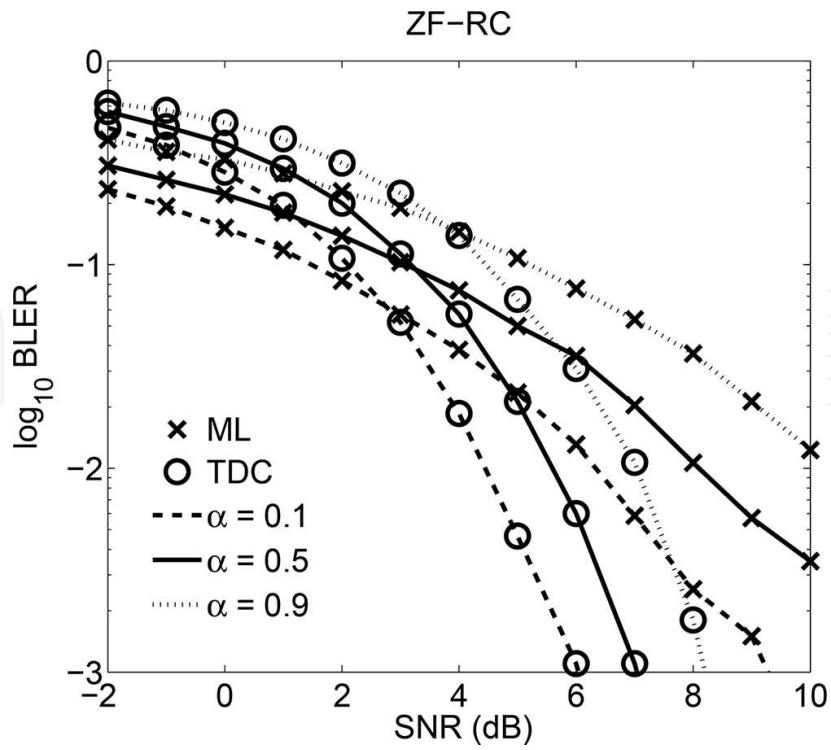


Figure 7. BLER comparison of the ML/TDC techniques with ZF, RC shaped filter and roll-off factor $\alpha = [0.1, 0.5$ and $0.9]$.

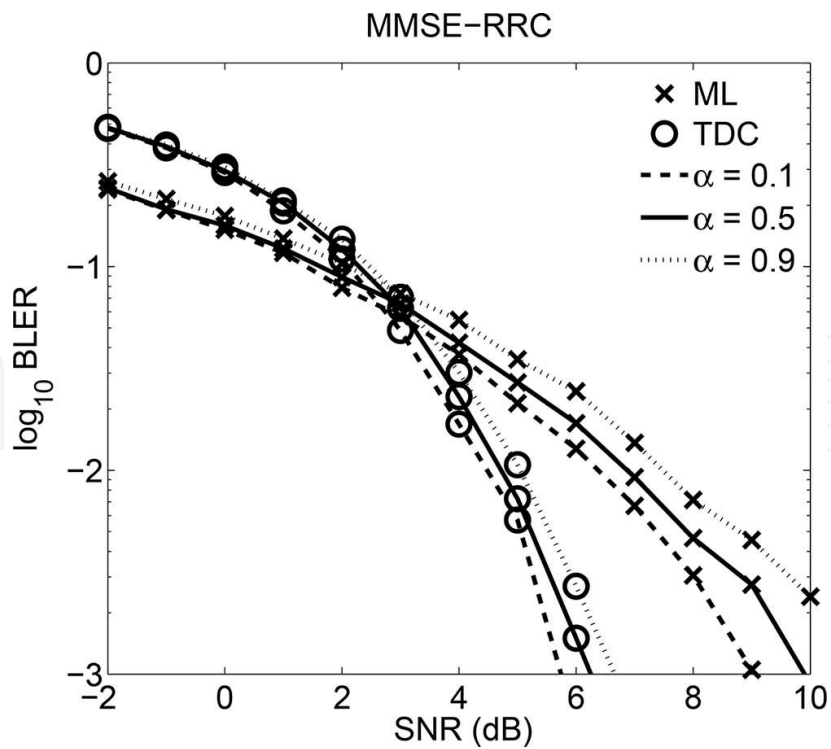


Figure 8. BLER comparison of the ML/TDC techniques with MMSE, RRC shaped filter and roll-off factor $\alpha = [0.1, 0.5$ and $0.9]$.

Figure 7 shows similar results for an RC shaped filter. Results in **Figures 6** and **7** show that the detection performance of both the ML and TD techniques is greatly influenced by the choice of the roll-off factor of each form of transmit filter. Results in **Figures 6** and **7** also show that the TDC techniques improve detection performance compared with the ML method.

In **Figures 6** and **7**, it can be seen that detection performance is degraded as the roll-off value is increased from 0.1 to 0.9. This can be attributed to the increasing level of the inherent noise enhancement factor of the ZF scheme as the roll-off factor is increased, as suggested within a major 5G research study highlighted in [2]. The RC shaped filter produces a slightly improved detection performance compared with the RRC shaped filter due to less inherent ICI in the RC shaped filter compared with the RRC filter, as suggested in [18].

4.2.2. Detection performance with MMSE-based GFDM receiver

Similarly, using the MMSE-based GFDM demodulation, **Figure 8** shows the BLER comparison with the use of an RRC shaped filter. **Figure 9** shows the same results using the RC shaped filter. Results in **Figures 8** and **9** show that the TDC technique improves detection performance in comparison with the ML method. Results in **Figures 8** and **9** also show that the detection performance is not significantly influenced by the value of the roll-off parameter of RC/RRC

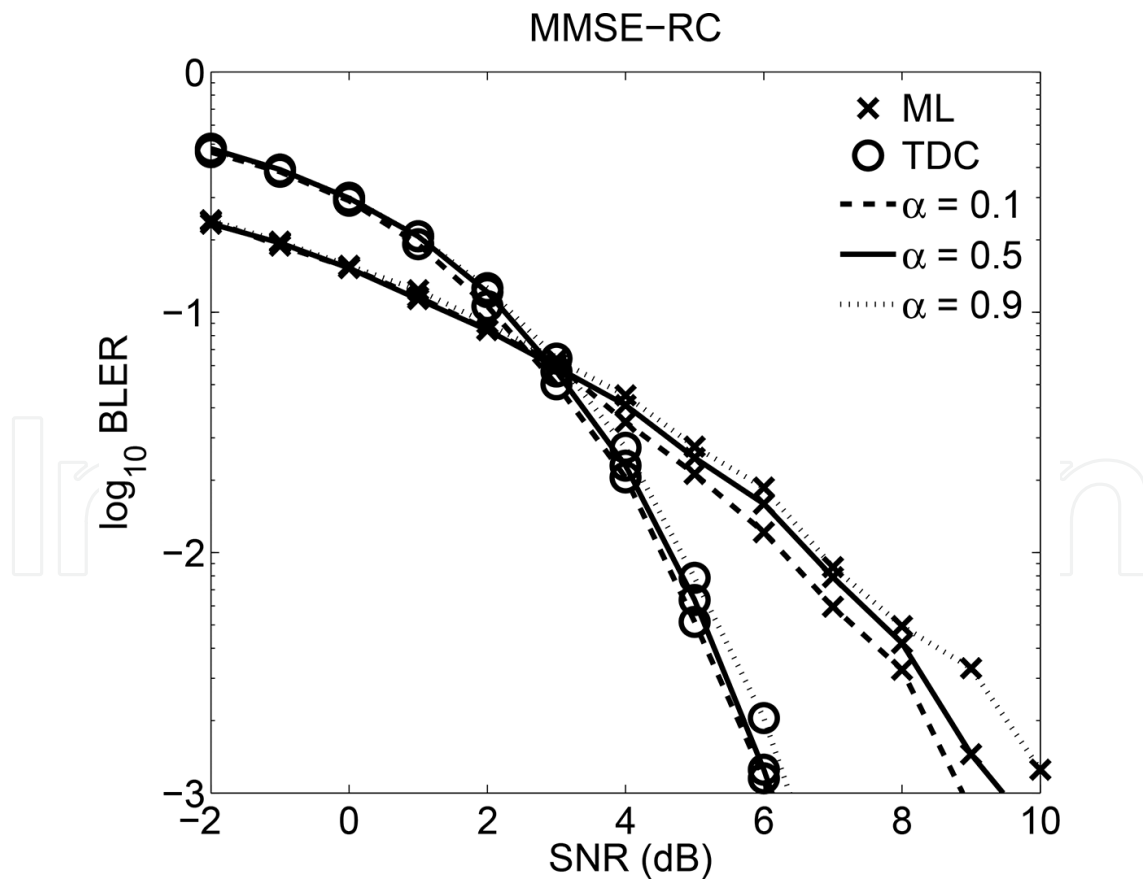


Figure 9. BLER comparison of the ML/TDC techniques with MMSE, RC shaped filter and roll-off factor $\alpha = [0.1, 0.5$ and $0.9]$.

Target BLER	GFDM receiver	Roll-off, α	Estimated SNR (dB)			
			RC		RRC	
			ML	TDC	ML	TDC
1%	ZF	0.1	6.4	4.6	6.5	4.6
		0.5	8.1	5.8	9.3	6.5
		0.9	>10.0	6.9	\gg 10.0	8.3
	MMSE	0.1	6.3	4.7	6.5	4.7
		0.5	6.7	4.8	6.9	4.9
		0.9	6.9	5.0	7.6	5.2
0.1%	ZF	0.1	9.4	6.2	8.8	6.0
		0.5	\gg 10.0	7.4	\gg 10.0	7.9
		0.9	\gg 10.0	8.6	\gg 10.0	10.0
	MMSE	0.1	8.9	5.9	9.1	6.3
		0.5	9.6	6.4	9.9	6.7
		0.9	>10.0	6.7	>10.0	6.9

Table 3. Estimated SNR (dB) at BLER levels of 1 and 0.1%.

shaped filter types. This is because the MMSE scheme produces no inherent noise enhancement. It is important to note that similar observations were also highlighted within a recent study found in [19].

4.2.3. Estimated SNR at target BLER of 1 and 0.1%

Table 3 shows the approximate SNR (in dB) required to achieve, for example, target BLER levels of 1 and 0.1%.

In summary, presented results in **Figures 6–9** support existing observations on the effects of filter shapes and the type of GFDM demodulation technique on the detection performance of the GFDM system. These results also show that the TDC technique has a robust detection performance capability and is potentially applicable in 5G systems.

5. Conclusions

This chapter introduced a TDC detection technique for SCI decoding and presented its detection performance using the GFDM architecture for 5G systems. Unlike the ML method of SCI detection, the TDC scheme requires no channel estimation and has no extra system overhead associated with channel estimation. It is shown that the TDC technique improves detection performance when compared with the conventional ML method.

With the ZF-based receiver, the BLER performance of the TDC technique is degraded as the roll-off value of the RC and RRC shaped filter is increased from 0.1 to 0.9. However, with the MMSE receiver, the detection performance of the TDC technique is relatively similar for different filter roll-off values. Hence, with the ZF-based receiver, the detection performance of the TDC technique is largely influenced by the choice of the roll-off value of the transmit filter. Furthermore, with the ZF-based receiver, the RC shaped transmit filter improved the BLER performance of the TDC technique compared with the RRC shaped filter of the same roll-off factor. Therefore, the TDC technique is a viable and an attractive SCI decoding solution for 5G systems.

Acknowledgements

We would like to thank Dr. Funmilayo Ogunkoya of the Electrical and Electronics Engineering department of Obafemi Awolowo University (OAU), Nigeria, for her support and insight towards producing some of the presented simulation results.

Author details

Saheed A. Adegbite^{1*} and Brian G. Stewart²

*Address all correspondence to: sa.adegbite@gmail.com

1 School of Engineering and Built Environment, Glasgow Caledonian University, Glasgow, UK

2 Department of Electronics and Electrical Engineering, University of Strathclyde, Glasgow, UK

References

- [1] 3GPP TSG-RAN R1-162248. Waveform for the next generation radio interface, 2016.
- [2] N. Michailow, M. Matthé, I. S. Gaspar, A. N. Caldevilla, L. L. Mendes, A. Festag, and G. Fettweis. Generalized frequency division multiplexing for 5th generation cellular networks. *IEEE Transactions on Communications*, 62(9):3045–3061, 2014.
- [3] 3GPP Technical Specification (TS) 36.211 v12.0.0. Evolved universal terrestrial radio access (E-UTRA); Physical Channels and Modulation, 2013.
- [4] S. A. Adegbite, S. G. McMeekin, and B. G. Stewart. Improved PCFICH decoding in LTE systems. In *The 21st IEEE International Workshop on Local and Metropolitan Area Networks*, IEEE, Beijing, China, pages 1–6, 2015.
- [5] S. A. Adegbite, S. G. McMeekin, and B. G. Stewart. A time-domain control signal detection technique for OFDM. *EURASIP Journal on Wireless Communications and Networking*, 2016(1):1–10, 2016.

- [6] S. J. Thiruvengadam and L. M. A. Jalloul. Performance analysis of the 3GPP-LTE physical control channels. *EURASIP Journal on Wireless Communications and Networking*, 2010(1):1–10, 2010.
- [7] S. Abbas, S. J. Thiruvengadam, and S. Susithra. Novel receiver architecture for LTE-A downlink physical control format indicator channel with diversity. *VLSI Design*, 2014:1–7, 2014.
- [8] I. S. Gaspar, L. L. Mendes, N. Michailow, and G. Fettweis. A synchronization technique for generalized frequency division multiplexing. *EURASIP Journal on Advances in Signal Processing*, 2014(1):1–10, 2014.
- [9] S. A. Adegbite, S. G. McMeekin, and B. G. Stewart. A selective control information detection scheme for OFDM receivers. *Telecommunication Systems*, 1–11, 2016. DOI: 10.1007/s11235-016-0154-6
- [10] S. Ehsanfar, M. Matthe, D. Zhang and G. Fettweis, "A Study of Pilot-Aided Channel Estimation in MIMO-GFDM Systems," WSA 2016; 20th International ITG Workshop on Smart Antennas, Munich, Germany, 2016, pp. 1–8.
- [11] H. Zamiri-Jafarian, H. Khoshbin, and S. Pasupathy. Time-domain equalizer for OFDM systems based on SINR maximization. *Communications, IEEE Transactions on*, 53(6):924–929, 2005.
- [12] J. Balakrishnan, R. K. Martin, and C. R. Johnson. Blind, adaptive channel shortening by sum-squared auto-correlation minimization (SAM). *IEEE Transactions on Signal Processing*, 51(12):3086–3093, 2003.
- [13] H. Minn and V. K. Bhargava. An investigation into time-domain approach for OFDM channel estimation. *IEEE Transactions on Broadcasting*, 46(4):240–248, 2000.
- [14] S. D. Stearns and D. R. Hush. *Digital Signal Processing with Examples in MATLAB®*, Second Edition. Taylor & Francis, Florida, USA, 2002.
- [15] Christian Walck. Handbook on statistical distributions for experimentalists. *Internal Report (SUF-PFY/96-01)*, University of Stockholm, Sweden, pages 138–139, 2007.
- [16] 3GPP Technical Specification (TS) 36.101 v12.0.0. Evolved universal terrestrial radio access (E-UTRA); User Equipment (UE) Radio Transmission and Reception, 2013.
- [17] S. Adegbite, B. G. Stewart, and S. G. McMeekin. Least squares interpolation methods for LTE system channel estimation over extended ITU channels. *International Journal of Information and Electronics Engineering*, 3(4):414–418, 2013.
- [18] B. M. Alves, L. L. Mendes, D. A. Guimaraes, and I. S. Gaspar. Performance of GFDM over frequency-selective channels-invited paper. In *Proceedings of International Workshop on Telecommunications*, Santa Rita do Sapucaí, Brazil, 2013.
- [19] N. Michailow, S. Krone, M. Lentmaier, and G. Fettweis. Bit error rate performance of generalized frequency division multiplexing. In *76th Vehicular Technology Conference (VTC Fall), 2012 IEEE*, IEEE, Quebec City, Canada, pages 1–5, 2012.